Journal of Power Sources 185 (2008) 1273–1283

Contents lists available at ScienceDirect

Journal of Power Sources

journal homepage: www.elsevier.com/locate/jpowsour

Modeling, control and simulation of an autonomous wind turbine/photovoltaic/fuel cell/ultra-capacitor hybrid power system

O.C. Onar[a,b], M. Uzunoglu[a,b,*], M.S. Alam[a]

[a] Department of Electrical and Computer Engineering, University of South Alabama, Mobile, AL 36688, USA
[b] Yildiz Technical University, Istanbul 34349, Turkey

ARTICLE INFO

Article history:
Received 17 June 2008
Received in revised form 25 August 2008
Accepted 26 August 2008
Available online 3 September 2008

Keywords:
Dynamic model
Fuel cell
Hybrid power generation
Photovoltaic
Ultra-capacitor
Wind power

ABSTRACT

This paper focuses on the combination of wind turbine (WT), photovoltaic (PV), fuel cell (FC) and ultra-capacitor (UC) systems for grid-independent applications. The dynamic behavior of the proposed hybrid system is tested under various wind speed, solar radiation and load demand conditions. The developed model and its control strategy exhibit excellent performance for the simulation of a complete day. In the simulation, the solar radiation and power demand data are based on real world measurements, while the wind speed data are quasi-real because it is simulated based on special wind speed generation algorithms.

1. Introduction

Renewable energy sources and conversion units such as PVs, WTs, and FCs have been found to be promising energy sources toward building a sustainable and environment friendly energy economy in the next decade. However, these renewable energy sources suffer from some deficiencies when used as stand-alone energy sources. The power generated by WT and PV systems is highly dependent on weather conditions. Natural variations in wind speed and sunlight causes power fluctuations in WT and PV systems, respectively. In addition, it is difficult to store the power generated by a PV or WT system for future use. To alleviate these problems, WT and PV sources can be integrated with other alternative systems using hybrid topologies. A hybrid power system consists of a combination of two or more energy sources, converters and/or storage devices. Thus, higher efficiency can be obtained by making the best use of their features while overcoming their limitations [1–4].

Alternate energy conversion systems such as PV panels and wind turbines can be combined with FC power plants to satisfy sustained load demands. An FC power plant uses hydrogen and oxygen to convert chemical energy into electrical energy. In this study, among the various types of FC systems, a Proton Exchange Membrane (PEM) FC power plant is used because PEMFC power plants have been found to be especially suitable for hybrid energy systems [5] since they have low operating temperature (80–1000 °C) and fast start-up. Currently, a 5 kW commercial PEMFC power plant is operational in the authors' lab. Moreover, PEMFC is suitable for using the hydrogen produced from the electrolysis of water since hydrogen is free from any carbon monoxide [1]. However, assisting an FC hybrid power plant with a parallel UC bank makes economic sense when satisfying the peak power demands or transient conditions since the UC bank supplies the extra power, thereby reducing the size and cost of the FC system. Ultra-capacitors are electrical energy storage devices (a few Farads to several thousand Farads per cell) with high power densities when compared to batteries [6]. Ultra-capacitor banks can be used for short-term energy storage due to their high cycling efficiency, convenience for charging/discharging, and additionally to meet the instantaneous load ripples/spikes. Besides, overloading fuel cell systems may cause gas starvation thus decreasing its performance and lifetime. As another feature, the load tracking delays and mismatches of the FCs should be compensated by an auxiliary system such as a battery or ultra-capacitor bank.

In this paper, the dynamic model, design and simulation of a new WT/PV/FC/UC autonomous hybrid system is proposed. To achieve autonomous operation and energy management, appropriate

* Corresponding author at: Department of Electrical Engineering, Yildiz Technical University, Istanbul 34349, Turkey. Tel.: +90 212 383 2441; fax: +90 212 259 4869.
E-mail addresses: conar@yildiz.edu.tr (O.C. Onar), uzunoglu@yildiz.edu.tr, mehmet_uzunoglu@yahoo.com (M. Uzunoglu), malam@usouthal.edu (M.S. Alam).

0378-7753/$ – see front matter © 2008 Elsevier B.V. All rights reserved.
doi:10.1016/j.jpowsour.2008.08.083

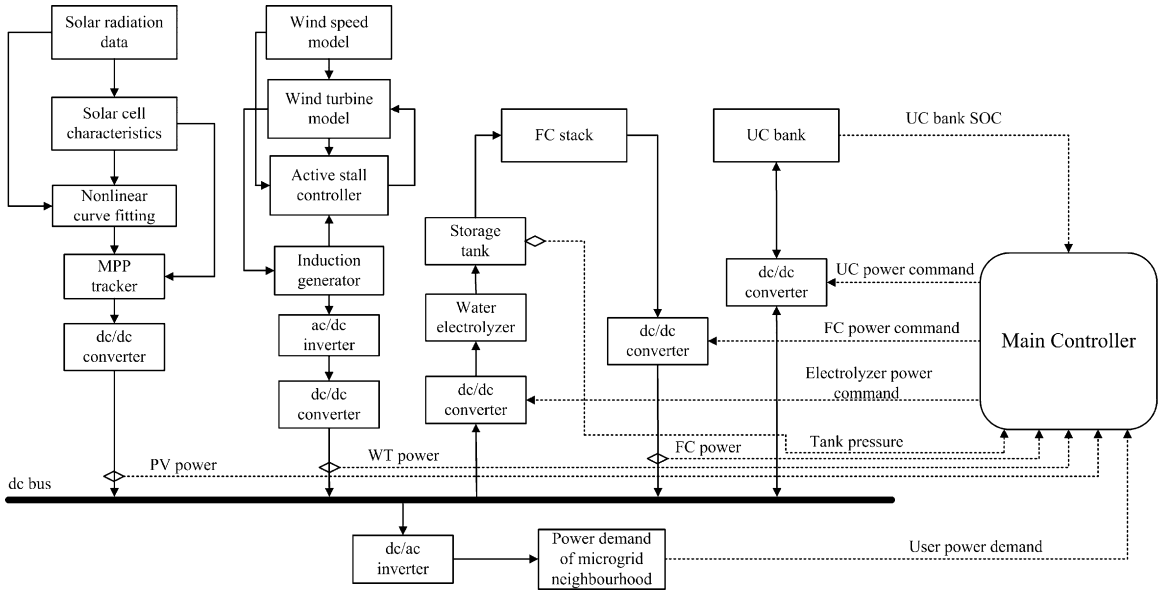

Fig. 1. Overall system configuration.

components and a control system is used to achieve adequate performance for the overall system. Here, the control system has been designed to draw the maximum available energy from the WT and PV sources. The excess power generated by renewable sources is used for UC charging and for the electrolyzer to produce hydrogen. When the energy generated from the WT and PV systems becomes insufficient with respect to the load demand, the stored hydrogen is fed to the FC system. The tracking mismatches of the FC system and the load demand exceeding the power generated by WT/PV/FC, is supplied by the UC bank. Using the developed model, the purpose of testing the overall performance of the complete system is achieved. Besides, the dynamic models of each component are integrated using the proposed topology with good performance. The model allows to design and size the hybrid system for a variety of loading and meteorological conditions. The developed model provides the integration of renewable energy systems with energy management strategy to overcome the deficiencies of each renewable system. Modeling and simulations are performed using MATLAB®, Simulink® and SimPowerSystems® [7–9] software packages and test results of the autonomous operation and energy management of the system show that this technique performs successfully.

2. System description and methodology

The overall configuration of the hybrid power generation system is shown in Fig. 1. The PV/FC/UC hybrid power system model reported in Ref. [10] and the dynamic PV system model reported in Ref. [11] are enhanced and integrated with the wind turbine, electrolyzer, storage, and load models. The primary energy sources of the system consist of a 10 kW WT and a 3 kW (peak) PV array. The excess energy with respect to the load requirement is used for UC charging and hydrogen production. The excess power demand of the user is supplied by the FC system up to 5 kW. When FC system is in operation, not only the excess demand over 5 kW but also the tracking mismatches and delays of the FC system are compensated by the UC bank.

The dc/dc converters depicted in Fig. 1 include two cascade connected converters. The bus side converters are used for bus voltage regulation and the source side converters are used for reference power tracking.

2.1. Wind speed, wind turbine and generator models

The Wind Turbine Blockset, developed in Ref. [12], is used in this study to realize and employ the wind speed, wind turbine and generator models. The model of the wind speed profile is based on Kaimal spectra [12]. This model takes into account the rotational turbulences and the tower shadow. The built-in band-limited white noise generator is used from Simulink and the wind speed is calculated as an averaging of the fixed-point wind speed over the whole rotor. The model of the wind turbine is based on the torque coefficient C_Q using a look-up table as a function of λ and θ for the variable pitch wind turbine. The torque coefficient C_Q is used to directly determine the aerodynamic turbine torque, given by

$$T_{\omega t} = 0.5\pi\rho R\upsilon^2 C_Q. \quad (1)$$

The parameters used in the wind turbine model are as follows:

C_Q	torque coefficient
R	blade radius
λ	tip speed ratio
ρ	air density
θ	pitch angle
υ	wind speed

An active stall controller is also employed to determine the optimal pitch angle and to limit the electrical output power to the nominal mechanical power. The cut-in and cut-off wind speed of the turbine is set to be 3 m s^{-1} and 15 m s^{-1}, respectively. The output torque of the wind turbine is used to drive the squirrel cage induction generator shaft. In the induction generator model, the steady-state voltage equations are used. Using this approach, the induction machine can be completely characterized in terms of steady-state values of the stator and rotor currents, phase angle, electromagnetic torque and electrical power. The electrical power which is supplied to the dc bus through the ac/dc and dc/dc converters is obtained from the stator windings of the induction generator. All detailed information on the components of WT system such as wind model, active stall controller, aerodynamic turbine model, and induction generator models can be found in Ref. [12]. The WT system configuration is given in Fig. 2.

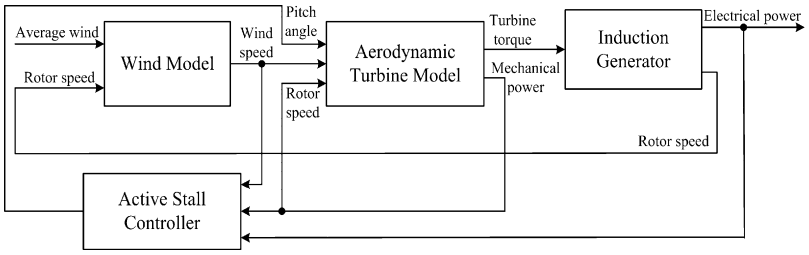

Fig. 2. WT system configuration.

2.2. PV system characteristics and model

A PV system consists of many cells connected in series and parallel to provide the desired output terminal voltage and current, and exhibits a nonlinear *I–V* characteristic [11,13]. Masoum et al. [11] introduced a model for Silicon solar PV panel. The PV cell equivalent model, which represents the dynamic nonlinear *I–V* characteristics of the PV system shown in Fig. 3, is used within the hybrid system as a controlled voltage source by utilizing it in the Simulink and SimPowerSystems toolboxes of MATLAB. The subsystems of the complete PV model are described in details in Ref. [10], which is a previous study of the authors, hence; those are not repeated in this study.

The parameters used in the mathematical modeling of the PV system are as follows:

a	ideality or completion factor
I_0	PV cell reverse saturation current [A]
I_{PV}	PV cell output current [A]
I_{sc}	short-circuit cell current [A]
k	Boltzmann's constant [JK^{-1}]
N_p	the number of parallel strings
N_s	the number of series cells per string
q	electron charge [C]
R_s	series resistance of PV cell [Ω]
T	PV cell temperature [K]
V_{PV}	terminal voltage for PV cell [V]

The output voltage characteristic of the PV system can be expressed as in Ref. [11] and [13],

$$V_{PV} = \frac{N_s akT}{q} \ln\left[\frac{I_{sc} - I_{PV} + N_p}{N_p I_0}\right] - \frac{N_s}{N_p} R_s I_{PV}. \quad (2)$$

The manufacturer's datasheet provides necessary information for most of the parameters of Eq. (2) [14]. The current–voltage characteristics of the PV array (for $N_p = 30$ and $N_s = 112$) are obtained according to the different short-circuit current values using Eq. (2) as shown in Fig. 4.

Using the current–voltage curves, the current–power curves can be obtained as shown in Fig. 5 to determine the maximum power to be drawn from the PV array under various short-circuit current values.

The maximum power output of the PV array varies according to solar radiation or load current. Therefore, a control system is needed to exploit the solar array more effectively as an electric power source by building a maximum power point tracker (MPPT) [15,16]. Different maximum power point tracker systems can be implemented. In this case, a computational approach is used involving the model of the nonlinear *I–V* characteristics of the solar panel. Based on the *I–V* characteristics, the corresponding maximum power points are computed for different load conditions as a function of cell short-circuit currents which varies as a function of the solar radiation. To determine the relationship between the solar radiation and short-circuit current, a curve fitting based computational method is employed. Then, an MPPT system, where the

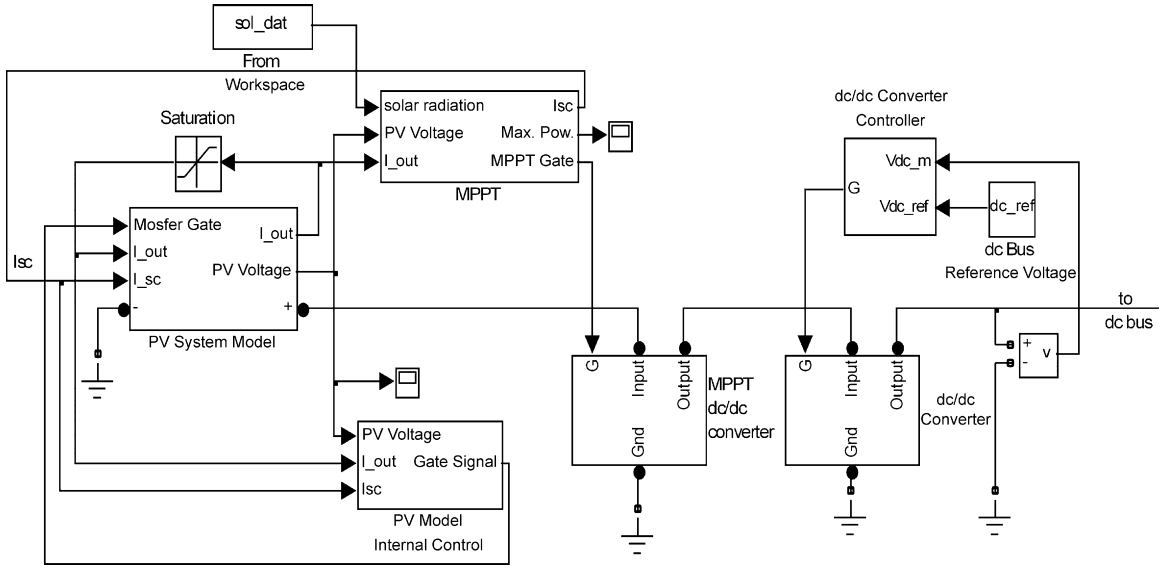

Fig. 3. PV system with MPPT, controllers and converters.

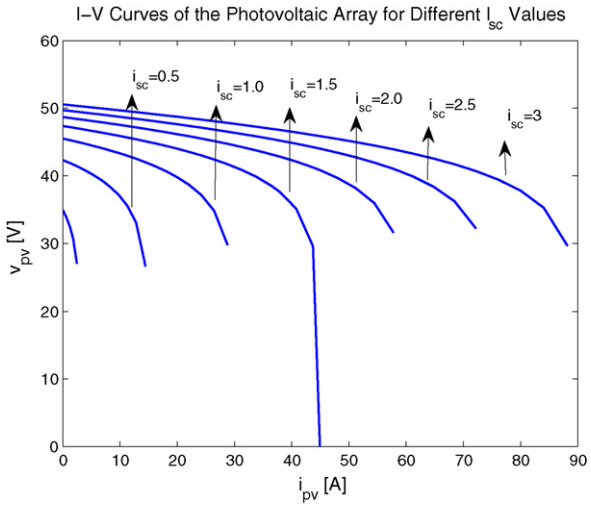

Fig. 4. Current–voltage curves for different short-circuit levels.

hardware part is based on a dc/dc converter is built to draw all the maximum available power from the PV generator.

The voltage based PV model exhibits the *I–V* characteristics of the PV system using a built-in dc/dc converter as shown in Fig. 3 (PV system model). The pulse width of the switching signal is determined using reference and measured voltages to represent the characteristic given in Eq. (2). Then, the pulse width command and the carrier signal are compared to obtain the switching PWM signals. The MPPT system calculates the maximum available power from the PV system, and then compares the calculated power with the actual drawn power for generating the switching signals of the dc/dc converter of the MPPT system. Another dc/dc converter cascaded after the MPPT converter which helps to keep the output voltage equal to the dc bus voltage.

The values of the PV system parameters are listed in Table 1.

2.3. PEMFC model

The PEMFC model described in Ref. [17] is modified using the relationship between output voltage and partial pressure of hydrogen, oxygen and water. The FC system model parameters used in this model are as follows:

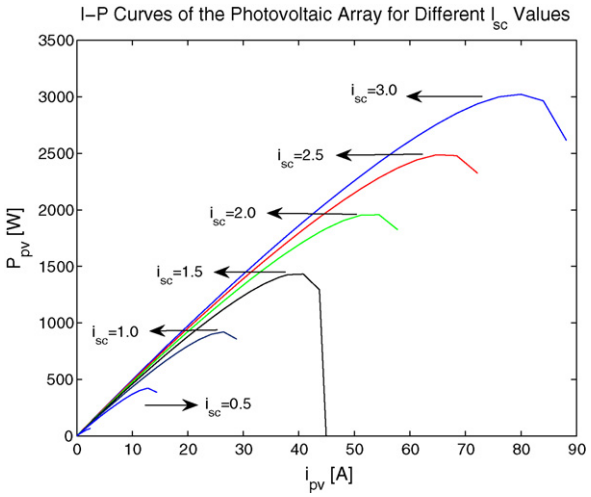

Fig. 5. Current–power curves for different short-circuit current values.

Table 1
PV system model parameters [11]

Specification	Value
The number of series cells per string (N_s)	30
The number of parallel cells per strings (N_p)	112
Ideality or completion factor (a)	1.9
Boltzmann's constant (k)	1.3805e−23 [J K^{-1}]
PV cell temperature (T)	298 [K]
Electron charge (q)	1.6e−19 C
Short-circuit cell current (representing insulation level) (I_{sc})	2.926 [A]
PV cell reverse saturation current (I_0)	0.00005 [A]
Series resistance of PV cell (R_s)	0.0277 [Ω]

B,C constants to simulate the activation over voltage in PEMFC system and [V]
CV conversion factor [kmol of hydrogen per kmol of methane]
E Nernst instantaneous voltage [V]
E_0 standard no load voltage [V]
F Faraday's constant [C (kmol)$^{-1}$]
I_{FC} FC system feedback current [A]
k_I PI gain
K_{an} anode valve constant [$\sqrt{\text{kmol kg}}$(atm s)$^{-1}$]
K_{H_2} hydrogen valve molar constant [$\sqrt{\text{kmol kg}}$(atm s)$^{-1}$]
K_{H_2O} water valve molar constant [$\sqrt{\text{kmol kg}}$(atm s)$^{-1}$]
K_{O_2} oxygen valve molar constant [$\sqrt{\text{kmol kg}}$(atm s)$^{-1}$]
K_r modeling constant [kmol (s A)$^{-1}$]
M_{H_2} molar mass of hydrogen (kg kmol^{-1})
N_0 number of series fuel cells in the stack
p_{H_2} hydrogen partial pressure [atm]
p_{H_2O} water partial pressure [atm]
p_{O_2} oxygen partial pressure [atm]
q_{H_2} molar flow of hydrogen [kmol s^{-1}]
q_{O_2} input molar flow of oxygen [kmol s^{-1}]
$q_{methane}$ methane flow rate [kmol s^{-1}]
$q_{H_2}^{in}$ hydrogen input flow [kmol s^{-1}]
$q_{H_2}^{out}$ hydrogen output flow [kmol s^{-1}]
$q_{H_2}^{r}$ hydrogen flow that reacts [kmol s^{-1}]
$q_{H_2}^{req}$ amount of hydrogen flow required to meet the load change [kmol s^{-1}]
R universal gas constant [(1 atm) (kmol K)$^{-1}$]
R^{int} FC internal resistance [Ω]
r_{H-O} the hydrogen–oxygen flow ratio
T absolute temperature [K]
U utilization rate
V_{an} volume of the anode [m^3]
V_{cell} dc output voltage of FC system [V]
τ_{H_2} hydrogen time constant [s]
τ_{O_2} oxygen time constant [s]
τ_{H_2O} water time constant [s]
η_{act} activation over voltage [V]
η_{ohmic} ohmic over voltage [V]

The relationship between the molar flow of any gas (hydrogen) through the valve and its partial pressure inside the channel can be expressed as [18]

$$\frac{qH_2}{pH_2} = \frac{K_{an}}{\sqrt{M_{H_2}}} = K_{H_2}. \quad (3)$$

For hydrogen molar flow, there are three significant factors: hydrogen input flow, hydrogen output flow, and hydrogen flow during the reaction [18]. The relationship among these factors can be

expressed as

$$\frac{d}{dt}p_{H_2} = \frac{RT}{V_{an}}(q_{H_2}^{in} - q_{H_2}^{out} - q_{H_2}^{r}). \quad (4)$$

According to the basic electrochemical relationship between the hydrogen flow and the FC system current, the flow rate of reacted hydrogen is given by [18]

$$q_{H_2}^{r} = \frac{N_0 N_s I_{FC}}{2F} = 2K_r I_{FC}. \quad (5)$$

Using Eqs. (3) and (5), and applying Laplace transform, the hydrogen partial pressure can be obtained in the s domain as [19]

$$p_{H_2} = \frac{1/K_{H_2}}{1 + \tau_{H_2} s}(q_{H_2}^{in} - 2K_r I_{FC}), \quad (6)$$

where

$$\tau_{H_2} = \frac{V_{an}}{K_{H_2} RT}. \quad (7)$$

Similarly, water partial pressure and oxygen partial pressure can be obtained. The polarization curve for the PEMFC is obtained from the sum of the Nernst's voltage, the activation over voltage, and the ohmic over voltage. Assuming certain temperature and oxygen concentration, the FC output voltage may be expressed as [17,20]

$$V_{cell} = E + \eta_{act} + \eta_{ohmic}, \quad (8)$$

where

$$\eta_{act} = -B \ln(CI_{FC}) \quad (9)$$

and

$$\eta_{ohmic} = -R^{int} I_{FC}. \quad (10)$$

Now, the Nernst's instantaneous voltage may be expressed as [17]

$$E = N_0 \left[E_0 + \frac{RT}{2F} \log \left[\frac{p_{H_2} \sqrt{P_{O_2}}}{p_{H_2O}} \right] \right]. \quad (11)$$

The FC system consumes hydrogen according to the power demand. The hydrogen is obtained from the high-pressure hydrogen tanks. During operational conditions, to control hydrogen flow rate according to the output power of the FC system, a feedback control strategy is utilized. To achieve this feedback control, FC current from the output is taken back to the input while converting the hydrogen into molar form [17,21]. The amount of hydrogen available from the hydrogen tank is given by

$$q_{H_2}^{req} = \frac{N_0 N_s I_{FC}}{2FU}. \quad (12)$$

Depending on the FC system configuration, and the flow of hydrogen and oxygen, the FC system produces the dc output voltage. The hydrogen–oxygen flow ratio r_{H-O} in the FC system determines the oxygen flow rate [17].

The values of the FC system parameters are listed in Table 2.

2.4. Ultra-capacitor model

The parameters used in the mathematical modeling of the UC are as follows:

C	capacitance [F]
$C_{UC\text{-}total}$	the total UC system capacitance [F]
EPR	equivalent parallel resistance [Ω]
ESR,R	equivalent series internal resistance [Ω]
E_{UC}	the amount of energy drawn from the UC bank [Ws]
n_s	the number of capacitors connected in series
n_p	the number of series strings in parallel

Table 2
FC system model parameters

Specification	Value
Activation voltage constant (B)	0.04777 [A^{-1}]
Activation voltage constant (C)	0.0136 [V]
Conversion factor (CV)	2
Faraday's constant (F)	96484600 [C $kmol^{-1}$]
Hydrogen time constant (τ_{H_2})	3.37 [s]
Hydrogen valve constant (K_{H_2})	4.22×10^{-5} [kmol (s atm)$^{-1}$]
Hydrogen–oxygen flow ratio (r_{H-O})	1.168
K_r constant = No/4F	2.2802×10^{-7} [kmol (s A)$^{-1}$]
Methane reference signal ($Q_{methref}$)	0.000015 [kmol s^{-1}]
No load voltage (Eo)	0.8 [V]
Number of cells (No)	88
Number of stacks (N_S)	1
Oxygen time constant (τ_{O_2})	6.74 [s]
Oxygen valve constant (k_{O_2})	2.11×10^{-5} [kmol (s atm)$^{-1}$]
FC system internal resistance (R_{int})	No × 0.00303 [Ω]
FC absolute temperature (T)	343 [K]
Universal gas constant (R)	8314.47 [J (kmol K)$^{-1}$]
Utilization factor (U)	0.8
Water time constant (τ_{H_2O})	18.418 [s]
Water valve constant (K_{H_2O})	7.716×10^{-6} [kmol (s atm)$^{-1}$]

$R_{UC\text{-}total}$	the total UC system resistance [Ω]
T	time [s]
$V(t)$	the voltage at time t [V]
V_i	the initial voltage before discharging starts [V]
V_f	the final voltage after discharging ends [V]

Fig. 6 shows the classical equivalent circuit of the UC unit. The model consists of a capacitance (C), an equivalent series resistance (ESR, R) representing the charging and discharging resistance, and an equivalent parallel resistance (EPR) representing the self-discharging losses [21,22]. The EPR models the leakage effects and only impacts long-term energy storage performance of the UC [23,24]. The voltage state of an UC (i.e., RC circuit) with a capacitance C draining charge into a resistance R may be expressed as [25]

$$V(t) = V_i \exp\left(-\frac{t}{RC}\right). \quad (13)$$

The RC time constant determines the effective period of the charging and discharging processes for some initial voltage on the capacitor [25]. The state of charge (SOC) of an UC bank is the available energy capacity expressed as a percentage of its rated energy capacity which is related to its voltage. The amount of energy drawn from the UC bank is directly proportional to the capacitance and the change in terminal voltage [23,6], which is expressed as

$$E_{UC} = \frac{1}{2}C(V_i^2 - V_f^2). \quad (14)$$

The effective specific energy for a prescribed load can be supplied by various UC bank configurations. In practical applications, the required amount of terminal voltage and energy or the capacitance of UC storage system can be built using multiple UCs in series

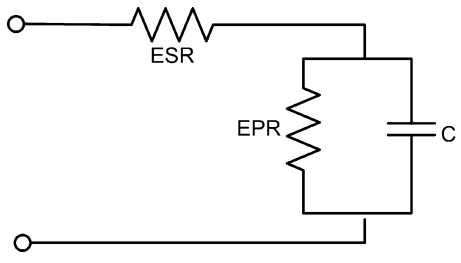

Fig. 6. Classical equivalent model for the UC unit.

Table 3
Maxwell Boostcap BMOD2600-48EA ulta-capacitor specifications

Specification	Value
Capacitance	144 [F]
Voltage	48.6 [V]
ESR, dc	11 [mΩ]
ESR @ 1 kHz	6.8 [mΩ]
Thermal resistance	0.27 [°C W^{-1}]
Short-circuit current	4800 [A]
Energy density (max)	3.40 [W h kg^{-1}]
Power density	2600 [W kg^{-1}]
Volume	13.4 [L]
Mass	13.5 [kg]

and parallel. The terminal voltage determines the number of capacitors which must be connected in series to form a bank and the total capacitance determines the number of capacitors which must be connected in parallel in the bank. The total system resistance and the total system capacitance of the UC bank can be calculated as [21,23]

$$R_{\text{UC-total}} = n_{\text{s}} \frac{\text{ESR}}{n_{\text{p}}}, \tag{15}$$

$$C_{\text{UC-total}} = n_{\text{p}} \frac{C}{n_{\text{s}}}. \tag{16}$$

In this research, Maxwell Technologies Boostcap® BMOD2600-48EA type ultra-capacitor bank is used which is currently operational in the authors' lab. The reasons for selecting this module are the ultra low internal resistance, low RC time constant and high power performance. In this study, 4 parallel UC modules are used, where each module includes 18 UC units connected in series. The specifications of the UC bank [26] is given in Table 3.

2.5. Electrolyzer and storage models

Water can be decomposed into its elementary components by passing electric current between two electrodes separated by an aqueous electrolyte [27–29]. The electrochemical reaction of water electrolysis is given by

$$\text{H}_2\text{O}_{(\text{liquid})} + \text{electrical energy} \Rightarrow \text{H}_2 + \frac{1}{2}\text{O}_2. \tag{17}$$

The Electrolyzer model involves the following parameters:

F	Faraday constant [C kmol^{-1}]
i_{e}	electrolyzer current [A]
n_{c}	the number of electrolyzer cells in series
η_{F}	Faraday efficiency
n_{H_2}	produced hydrogen moles per second [mol s^{-1}]

According to Faraday's law, hydrogen production rate of an electrolyzer cell is directly proportional to the electrical current in the equivalent electrolyzer circuit [27], which can be expressed as

$$n_{\text{H}_2} = \frac{\eta_{\text{F}} n_{\text{C}} i_{\text{e}}}{2F}. \tag{18}$$

The ratio between the actual and the theoretical maximum amount of hydrogen produced in the electrolyzer is known as Faraday efficiency. Assuming that the working temperature of the electrolyzer is 40 °C, Faraday efficiency is expressed by Refs. [27,29]

$$\eta_{\text{F}} = 96.5\, e^{(0.09/i_{\text{e}} - 75.5/i_{\text{e}}^2)}. \tag{19}$$

According to Eqs. (18) and (19), a simple electrolyzer model is developed using Simulink.

The amount of hydrogen required by the PEMFC is sent directly from the electrolyzer system according to the relationship between the output power and the hydrogen requirement of the PEMFC system. The remaining amount of hydrogen, i.e., the difference

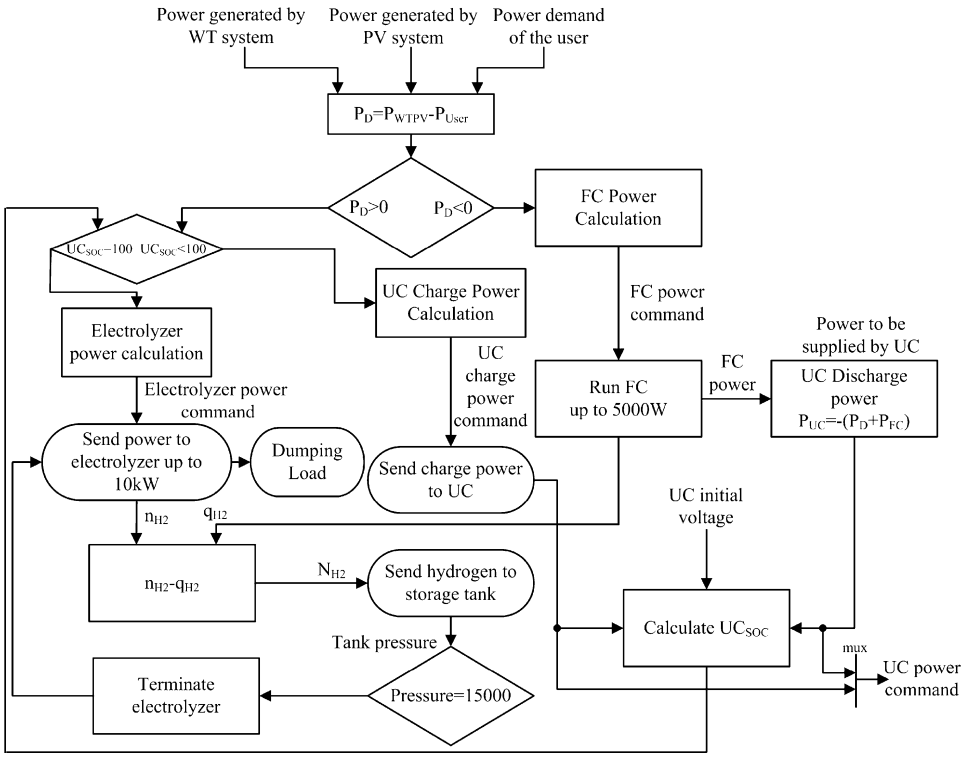

Fig. 7. The general decision algorithm used in the main controller.

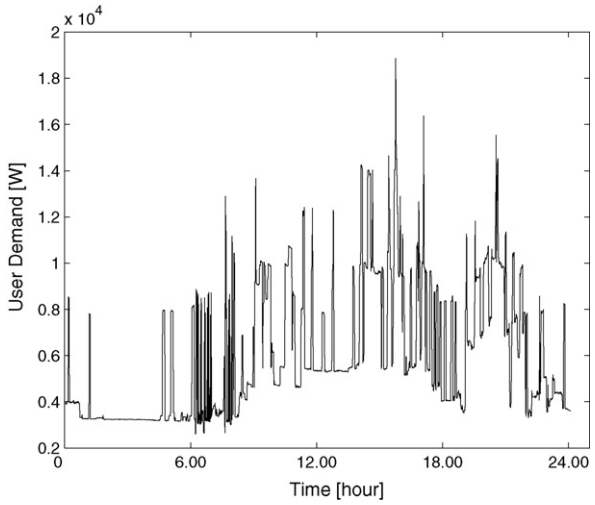

Fig. 8. Power demand of the micro-grid neighborhood consisting of 3 residential units.

between the produced and consumed hydrogen is sent to the storage tank.

One of the hydrogen storage techniques is physical hydrogen storage, which involves using tanks to store either compressed hydrogen gas or liquid hydrogen. The hydrogen storage model is based on Eq. (20) and it directly calculates the tank pressure using the ratio of hydrogen flow to the tank. The produced hydrogen is stored in the tank, whose system dynamics can be expressed as [30]

$$P_b \hat{-} P_{bi} = z\frac{N_{H_2} R T_b}{M_{H_2} V_b}. \quad (20)$$

The parameters used in the hydrogen storage system are listed below:

M_{H_2}	Molar mass of hydrogen [kg kmol^{-1}]
N_{H_2}	hydrogen moles per second delivered to the storage tank [kmol s^{-1}]
P_b	pressure of tank [Pa]
P_{bi}	Initial pressure of the storage tank [Pa]
R	universal (Rydberg) gas constant [J (kmol K)$^{-1}$]
T_b	operating temperature [K]
V_b	volume of the tank [m^3]
z	compressibility factor as a function of pressure

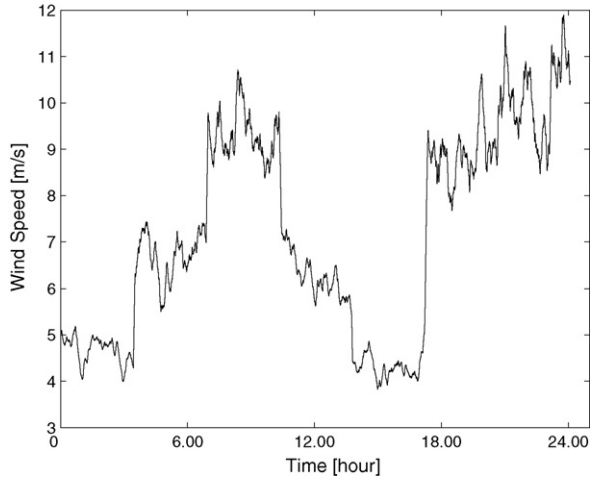

Fig. 9. Wind speed profile.

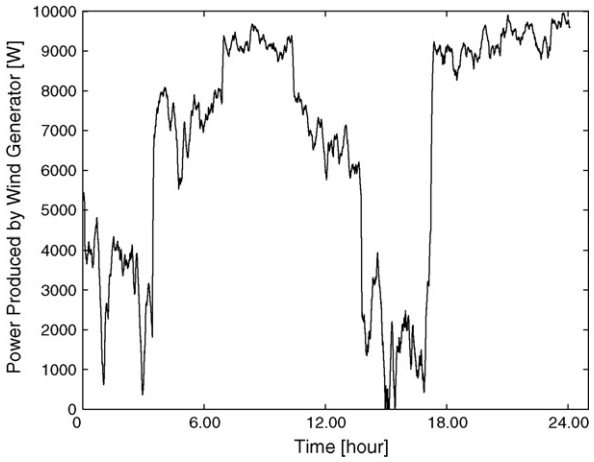

Fig. 10. Power produced by the wind generator.

The compression dynamics and the compression energy requirements are not considered in our calculations. All auxiliary power requirements such as pumps, valves and compression motors are ignored in the dynamic model since their investigation is out of the paper's scope.

2.6. Energy management and control strategy

A main controller is employed for the entire energy measurement and management purposes. The main controller provides the autonomous operation with the required measurements, decisions and controls by collecting data through the sensors and producing the commands for the power converters connected to the inputs/outputs of the components used in the hybrid system. The operating strategies used in the main controller are as follows:

- The use of power generated by the PV and WT systems has priority in satisfying power demand over that provided by the FC system or by the UC bank.
- If the total power generated by the PV and WT systems is higher than the demand, the additional power will be used to charge the UC bank.
- After charging the UC bank, the remaining power is used for the electrolyzer through a power converter to generate hydrogen.

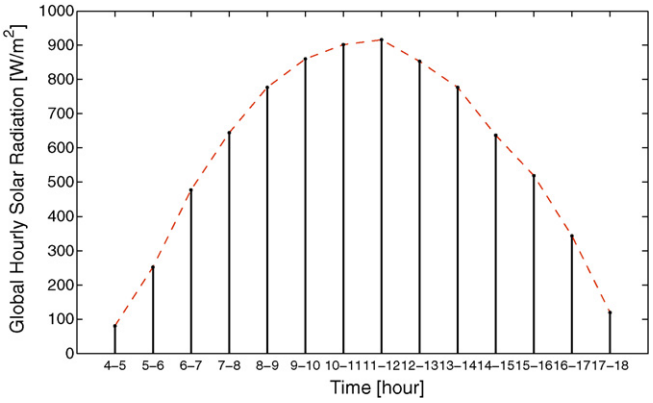

Fig. 11. Global hourly solar radiation.

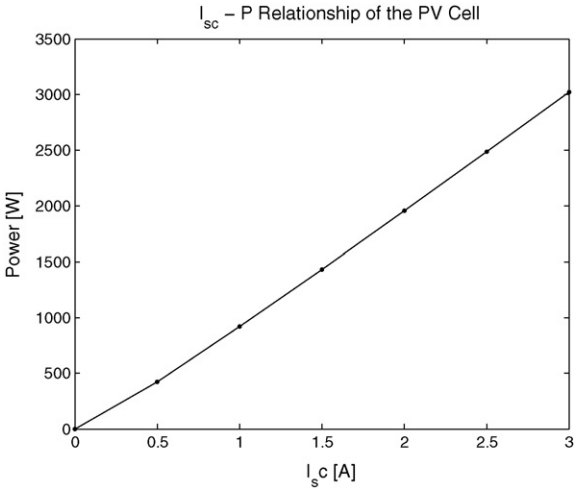

Fig. 12. Short-circuit current versus power variation.

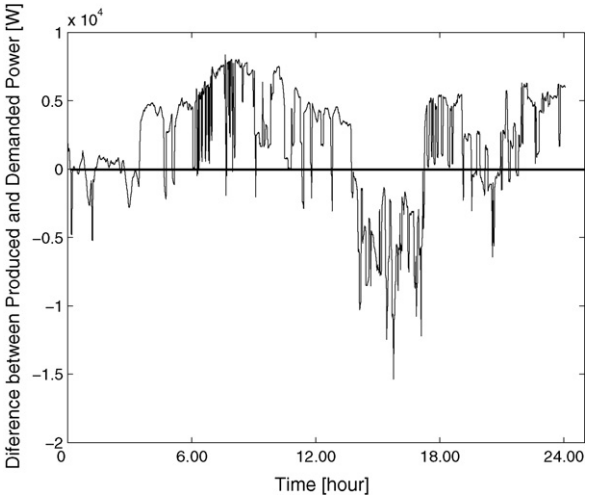

Fig. 14. The difference between the load power and generated power (PV + WT).

- The electrolyzer is kept in operation as long as available power exists and the tank pressure does not exceed the prescribed value of 15,000 Pa. The electrolyzer maximum power is also set to 10 kW. The additional power generated by the WT and PV systems can be transferred to the electrolyzer up to the 10 kW limit.
- Dumping power is necessary if the UC bank is fully charged and the electrolyzer power is at 10 kW limit.
- If the total electric power generated by the PV and WT systems is less than the demand, power will be supplied from the FC system up to the maximum 5 kW limit. If the load demand exceeds the power generated by WT/PV/FC combination, the difference is supplied by the UC bank.
- The UC bank not only provides the excess power demand over 5 kW, but also compensates the tracking mismatches and delays of the FC system which has relatively slow response time.
- The UC bank maximum voltage is set to be its nominal voltage of 48.6 V and its minimum voltage is set to be 25% of full state of charge (SOC) to avoid overcharging and deep discharging.

To implement the aforementioned power management strategy, appropriate power control systems are used at relevant points and the total system components are integrated. The block diagram of the main controller is illustrated in Fig. 7.

3. Results and discussions

In the simulation process, the aim is to observe the proposed system's behavior over a long period of time including day and night cases as well as low or no wind conditions. The load profile, wind speed variation and solar radiation profiles are all used to test the performance of the proposed hybrid system for a typical day of the neighborhood.

The 5 kW PEMFC system currently operated in our laboratory feeds a 500 ft^2 house. Energy consumption varies from house to house, but to simulate a real-world scenario, load profiles are also obtained from a neighborhood comprising of three houses, where each house is approximately 2500 ft^2 and includes all household electrical devices. The load profile of the micro-grid neighborhood is illustrated in Fig. 8.

The wind speed profile is generated by the wind speed model described in Section 2.1 and the hourly wind speed profile is depicted in Fig. 9, which yields the power generated by WT as shown in Fig. 10.

The hourly averaged global solar radiation on a horizontal surface ($W\,m^{-2}$) is taken from Ref. [31], where the record coordinates are: Latitude 41°10′ North and Longitude 40°20′ East. The experimental solar radiation data which is recorded by the regional meteorological station in the month of June is given in Fig. 11.

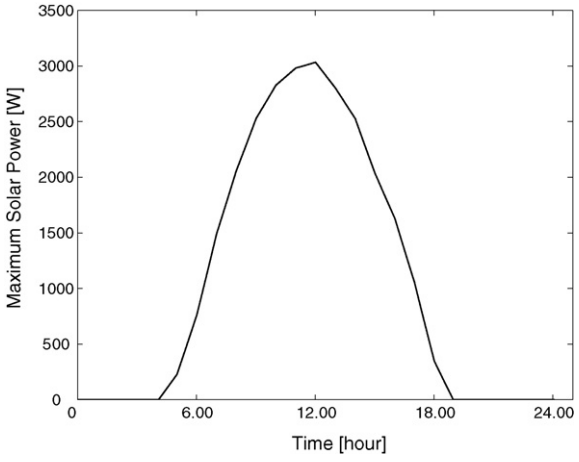

Fig. 13. Hourly power drawn from the solar system.

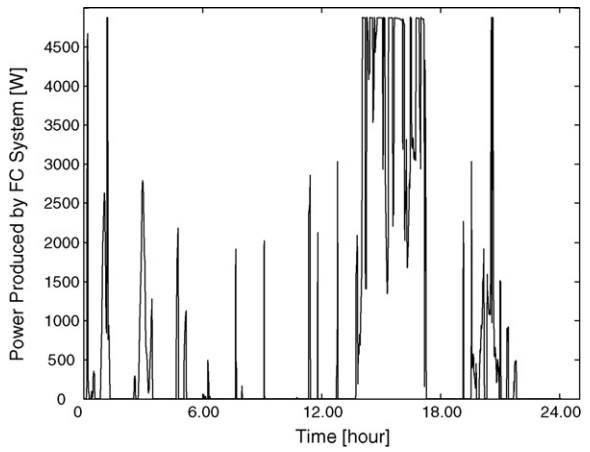

Fig. 15. Power produced by the FC system.

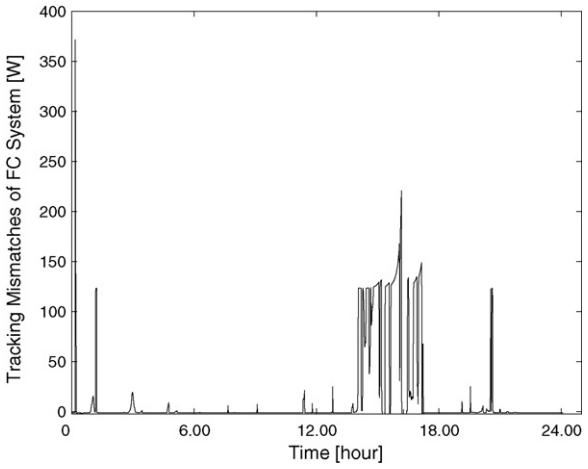

Fig. 16. Tracking mismatches of the FC system.

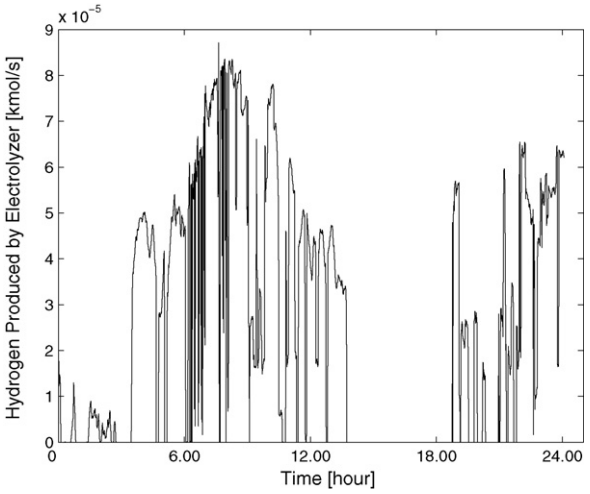

Fig. 18. Amount of hydrogen produced by the electrolyzer.

Using the nonlinear curve fitting based computation, the relationship between the solar radiation and the short-circuit current is obtained. Then using the maximum power points for different short-circuit values given in Fig. 5, the short-circuit current and the maximum power relationship are obtained as shown in Fig. 12. It is evident from Fig. 12 that the short-circuit current varies almost linearly with the solar radiation.

The maximum power values are used in the MPPT dc/dc converter as power commands and the maximum power drawn from the PV system to the dc bus is obtained as illustrated in Fig. 13. From Fig. 13, we observe that in the early morning before 4:08 and in the evening after 19:38, the solar power is unavailable due to nonexistence of solar radiation. The maximum power from PV system can be transferred to the dc bus at about 12.02 in the noon.

As mentioned earlier, the use of power generated by the PV and WT systems has priority in satisfying load demand. Thus, the total power generated by the WT and PV systems is transferred to the dc bus directly. The difference between the power generated by WT and PV systems and the user power demand is demonstrated in Fig. 14. The positive regions of Fig. 14 are the additional power generated by PV and WT sources which is used for the UC charging and hydrogen production within the electrolyzer system. Furthermore, the negative regions are the exceeded power demands which are met by the FC system and UC bank discharge.

The FC system power command is obtained according to the negative regions of Fig. 14 (exceeded user demands) up to the 5 kW limit. The power produced by FC system is given in Fig. 15, which slightly differs from the power command due to the time constants and relatively slow response characteristic of the FC system. However, since the required hydrogen is not processed by a reformer and provided directly from the hydrogen tank, the reformation time delays are eliminated.

The tracking mismatches of the FC system are given in Fig. 16 which is supposed to be supplied by the UC bank. The power produced by the FC system shown in Fig. 15 corresponds to the amount of hydrogen flow to the FC system as depicted in Fig. 17. The amount of power transferred to the electrolyzer corresponds to the hydrogen flow from the electrolyzer to the storage tank as illustrated in Fig. 18.

The hydrogen produced by the electrolyzer and consumed by the FC system causes the pressure of the storage tank to vary as shown in Fig. 19. The pressure of the storage tank increases when the electrolyzer produces hydrogen, and the tank pressure decreases when the FC system uses the stored hydrogen.

The power supplied by the UC bank is shown in Fig. 20 which includes the exceeded load demand and the tracking mismatches (Fig. 16) of the FC system. Due to the scaling differences of Figs. 16 and 20, the low mismatches cannot be seen in Fig. 20. These

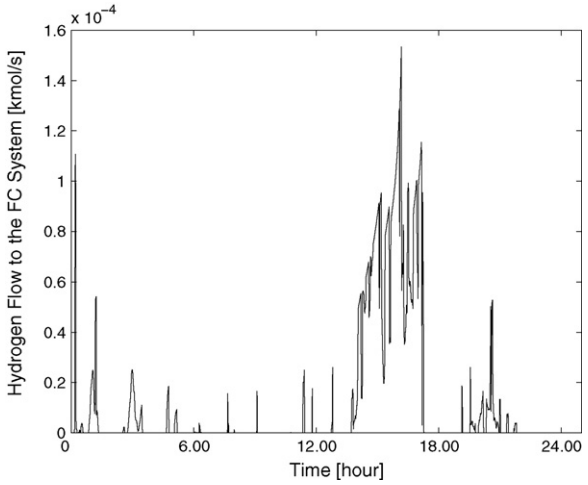

Fig. 17. Amount of hydrogen required by the FC system.

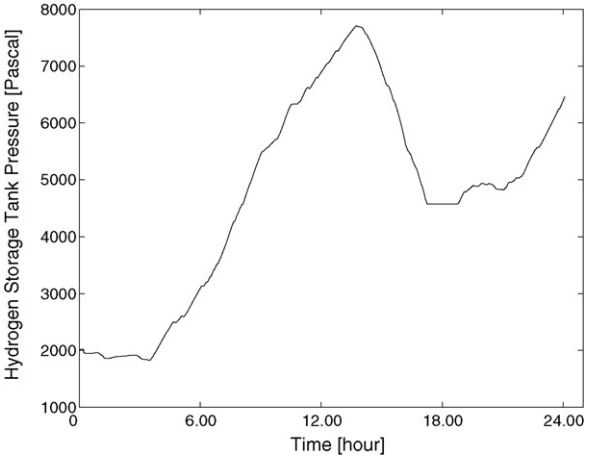

Fig. 19. The pressure variation of the hydrogen storage tank.

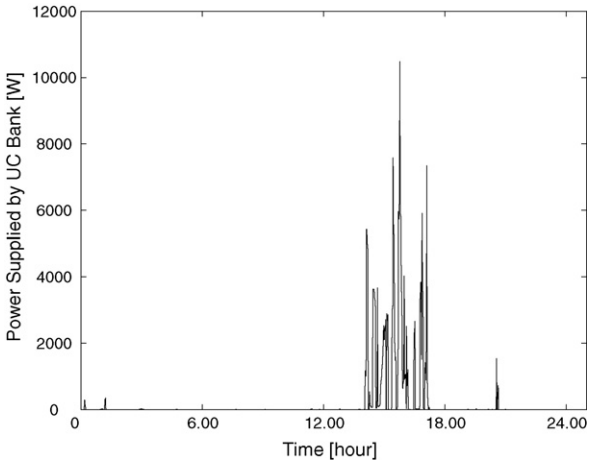

Fig. 20. Power supplied by UC bank including tracking delays and all mismatches.

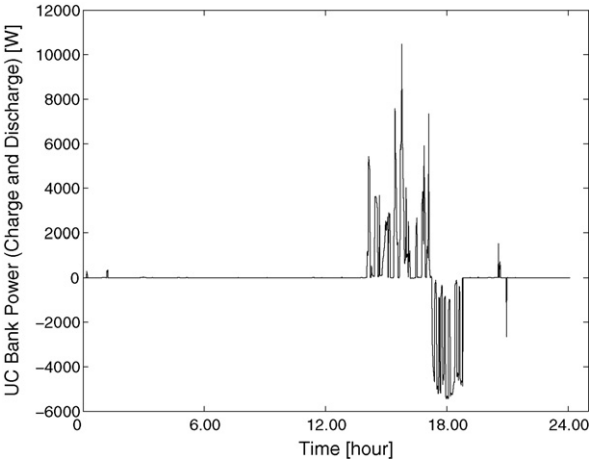

Fig. 21. UC bank charge and discharge power.

mismatches can be observed by zooming into the areas of interest of Fig. 20.

The charge and discharge power of the UC bank is recorded as shown in Fig. 21, where positive power region represents the power released by the UC bank and negative power region represents the power captured by the UC bank through the bi-directional dc/dc converter.

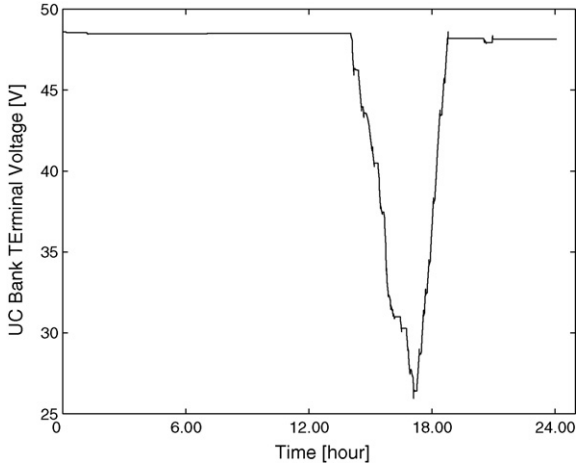

Fig. 22. UC bank terminal voltage.

The charging and discharging power of the UC bank corresponds to the terminal voltage variation as demonstrated in Fig. 22. From Fig. 22, it is obvious that the UC bank terminal voltage varies with the charge and discharge state of the UC bank within the limited values.

4. Conclusions

A novel WT/PV/FC/UC hybrid power system is designed and modeled for grid-independent applications. A detailed simulation model has been developed which allows designing and analyzing any WT/PV/FC/UC hybrid system with various power levels and parameters. The dynamic behavior of the hybrid system is tested under various wind speed, solar radiation and load demand conditions. The solar radiation and power demand data are based on real world records and the wind speed is artificially generated in the computer environment using a suitable algorithm.

The main contribution of this work is the hybridization of the renewable energy sources with FC systems using long and short-term storage strategies with appropriate power controllers and control strategy to build an autonomous system. The developed system and its control strategy exhibit excellent performance for the simulation of a complete day or longer periods of time. The proposed system can be used for non-interconnected remote areas or isolated cogeneration power applications as a reliable and technically feasible system.

Acknowledgement

This work was supported in part by the U.S. Department of Energy under Grant DE-FG02-05CH11295.

References

[1] K. Rajashekara, IEEE Trans. Ind. Appl. 41 (3) (2005) 682–689.
[2] K. Agbossou, M. Kolhe, J. Hamelin, T.K. Bose, IEEE Trans. Energy Convers. 19 (3) (2004) 633–640.
[3] A. Bilodeau, K. Agbossou, J. Power Sources 162 (2) (2006) 757–764.
[4] O.C. Onar, M. Uzunoglu, M.S. Alam, J. Power Sources 161 (1) (2006) 707–722.
[5] L. Gao, Z. Jiang, R.A. Daugal, J. Power Sources 130 (1–2) (2004) 202–207.
[6] A. Burke, J. Power Sources 91 (1) (2000) 37–50.
[7] M. Uzunoglu, A. Kizil, O.C. Onar, Her Yonu ile MATLAB (Proficiency in MATLAB, 2nd Edition), Turkmen Kitabevi, Istanbul, 2003.
[8] MATLAB Simulink Simulation and Model Based Design User's Guide, Version 6.3 [Online]. Available: http://www.mathworks.com/access/helpdesk/help/pdf_doc/simulink/sl_using.pdf.
[9] MATLAB SimPowerSystems for Use with Simulink User's Guide, Version 4.1.1 [Online]. Available: http://www.mathworks.com/access/helpdesk/help/pdf_doc/physmod/powersys/powersys.pdf.
[10] M. Uzunoglu, O.C. Onar, M.S. Alam, Modeling, control and simulation of a PV/FC/UC based hybrid power generation system for stand-alone applications, Renewable Energy, accepted for publication, DOI information: 10.1016/j.renene.2008.06.009.
[11] M.A.S. Masoum, H. Dehbonei, E.F. Fuchs, IEEE Trans. Energy Convers. 17 (4) (2002) 514–522.
[12] F. Iov, A.D. Hansen, P. Sørensen, F. Blaabjerg, Wind Turbine Blockset in MATLAB/Simulink (A Simulation Platform to Model, Optimize and Design Wind Turbines), Project Participants: Aalborg University Institute of Technology, RISØ National Laboratory, Support from Danish Energy Agency through Grant 1363/01-0013, 2004–2007.
[13] M. Veerachary, T. Senjyu, K. Uezato, IEEE Trans. Aerospace Electron. Syst. 38 (1) (2002) 262–270.
[14] Y. Sukamongkol, S. Chungpaibulpatana, W. Ongsakul, Renew. Energy 27 (2) (2002) 237–258.
[15] R. Chedid, S. Rahman, IEEE Trans. Energy Convers. 13 (1) (1998) 76–83.
[16] K. Kobayashi, H. Matsuo, Y. Sekine, IEEE Trans. Ind. Electron. 53 (1) (2006) 281–286.
[17] M.Y. El-Shark, A. Rahman, M.S. Alam, P.C. Byrne, A.A. Sakla, T. Thomas, J. Power Sources 138 (1–2) (2004) 199–204.
[18] J. Padulles, G.W. Ault, J.R. McDonald, J. Power Sources 86 (1–2) (2000) 495–500.
[19] L. Gao, R.A. Dougal, S. Liu, IEEE Trans. Power Electron. 20 (1) (2005) 236–243.
[20] J. Hamelin, K. Agbossou, A. Laperriere, F. Laurencelle, T.K. Bose, Int. J. Hydrogen Energy 26 (6) (2001) 625–629.

[21] K.-H. Hauer, Analysis tool for fuel cell vehicle hardware and software (controls) with an application to fuel economy comparisons of alternative system designs, Ph.D. Dissertation, Dept. Transportation Technology and Policy, University of California, Davis, 2001.
[22] R.M. Nelms, D.R. Cahela, B.J. Tatarchuk, IEEE Trans. Aerospace Electron. Syst. 39 (2) (2003) 430–438.
[23] R.L. Spyker, R.M. Nelms, IEEE Trans. Aerospace Electron. Syst. 36 (4) (2000) 1439–1443.
[24] R.L. Spyker, R.M. Nelms, IEEE Trans. Aerospace Electron. Syst. 36 (3) (2000) 829–836.
[25] B.E. Conway, Electrochemical Supercapacitors-Scientific Fundamentals and Technological Applications, Kluwer Academic/Plenum Publishers, New York, 1999, pp. 497–547.
[26] Maxwell Technologies, BOOSTCAP® Energy Storage Module BMOD2600-48EA (104567), User's Manual.
[27] M.J. Khan, M.T. Iqbal, Renew. Energy 30 (3) (2005) 421–439.
[28] O. Ulleberg, Stand-alone Power Systems for the Future: Optimal Design. Operation and Control of Solar-Hydrogen Energy Systems, Ph.D. Dissertation, Norwegian University of Science and Technology, 1998.
[29] K. Sapru, N.T. Stetson, S.R. Ovshinsky, Development of a Small Scale Hydrogen Production Storage System for Hydrogen Applications, presented at the Energy Conversion Engineering Conference, in Proc. The 32nd Intersociety, Honolulu, HI, USA, 1997, pp. 1947–1952.
[30] H. Gorgun, Int. J. Hydrogen Energy 31 (1) (2006) 29–38.
[31] K. Kaygusuz, T. Ayhan, Energy Convers. Manage. 40 (5) (1999) 545–556.